Morphological Analysis of Fenestrae in Arteries

Muhammad Moazzam Jawaid[3(✉)], Francisco Ramirez-Perez[2], Antoine Plumerault[1], Flora Quilichini[1], Jose Alonso Solis-Lemus[1], Luis Martinez-Lemus[2], and Constantino Carlos Reyes-Aldasoro[1]

[1] School of Mathematics, Computer Science and Engineering, City, University of London, London, UK
[2] Dalton Cardiovascular Research Center, University of Missouri, Columbia, MO, USA
[3] Mehran University of Engineering and Technology, Jamshoro, Pakistan
moazzam.jawaid@faculty.muet.edu.pk

Abstract. Cardiovascular disease (CVD) is worldwide cause of death. The morphological structure of one of the regions of arteries called the internal elastic lamina (IEL) is associated with the stiffness of arteries, especially the presence and characteristics of small holes called *fenestrae*. Structural analysis of the IEL as observed with multiphoton or confocal fluorescent microscopy is complicated, primarily due to is three-dimensional distribution along a series of z-stack slices. In addition, whilst the top slices of an artery cross long lamina sections, the bottom slices only cross short sections of the lamina and would be better observed in a different plane than that of the acquired image.

In this work, we describe a framework to analyse 3D stacks of arteries as observed with fluorescent multiphoton microscopy. We apply this framework to the study of arterial stiffness as inferred from the presence/absence of fenestra the IEL and their morphological characteristics. The framework assumes the arteries as cylinders, then performs a series of geometrical transformations to align the data in three dimensions. The IEL is segmented from the external elastic lamina (EEL) and then each lamina is projected to a plane from which the fenestrae of all slices can be analysed in a single 2D image. The fenestrae are segmented by filtering with a Laplacian of a Gaussian kernel with optimal parameters. The results were compared against manually segmented fenestrae and provided a classification accuracy of [98–99%] and Jaccard Index values in the range of [38–54%], which are comparable the variations of 3 independent manual segmentations. The code is available from the website https://github.com/reyesaldasoro/Arterial-Fenestrae.

1 Introduction

Cardiovascular disease (CVD) is worldwide cause of death and sometimes considered *world's top killer* [1]. Consumption of excess fat and carbohydrate, in some cases called *Western diet*, (WD) is associated with alterations in the structural

M. H. Miraz et al. (Eds.): iCETiC 2018, LNICST 200, pp. 273–282, 2018.
https://doi.org/10.1007/978-3-319-95450-9_23

characteristics of blood vessels and could lead to CVD. This WD is prevalent in some countries like the USA and has led to alarming increases in obesity and type II diabetes, risk factors to CVD [2]. Development of CVD and hypertension is even associated with exposure to adverse maternal environments e.g. Gestational diabetes mellitus (GDM) [3,4]. Vascular remodelling may contribute to the pathophysiology of vascular diseases and circulatory disorders [5,6]. One of the regions of particular interest in the structure of the terminal vascular bed is the internal elastic lamina (IEL) [7]. Remodelling is often associated with morphological changes in the IEL such as increased vascular elastin [8] or flow-induced arterial enlargement [9]. The IEL presents a characteristic formation of windows commonly called *fenestra* and its characteristics are important as in cases enlarged fenestra have been assumed to represent a weakness of the IEL and may contribute to microaneurysms [10].

Structural analysis of the IEL as observed with multiphoton or confocal fluorescent microscopy is complicated, primarily due to is three-dimensional distribution along a series of z-stack slices. It is common practice to analyse the IEL visually [5], and only a few regions of interest (ROI) in selected slices, and thus a large amount of information from the arteries, especially the region of the artery where the IEL is nearly perpendicular to the field of view, is not considered for analysis.

In this work, a framework for the analysis of IEL of arteries as observed with a multiphoton microscope is proposed. The main step of the framework is the projection of the artery, from a cylindrical structure to a 2D plane. In this way, all the regions of the artery can be observed in a single plane. The presence of the fenestrae in the two-dimensional IEL is analysed through intensity-based algorithms and validated against a manually-segmented ground truth. Finally, we apply the framework to compare two populations of different rats which provided statistical differences.

An additional advantage of the projection approach is that the lamina that resides outside the IEL, called the External Elastic Lamina (EEL) can also be projected and further analysed. Analysis of the EEL is beyond the scope of this work.

2 Materials and Methods

2.1 Data Sets

Details of acquisition and animals have been described previously [4] but briefly, mesenteric resistance arteries (MRA, 186–301 μm internal diameter) were harvested from spontaneously hypertensive rats (SHR, n = 4) and MRA segments from Wistar Kyoto rats (WKY, n = 4) following NIH and local Guidelines and Ethical Approvals. For illustration purposes, one femoral artery was also acquired (Set D in Fig. 2). Vessels were imaged using a Leica SP5 confocal/multiphoton microscope with a 63x/1.2 numerical aperture water objective. Alexa Fluor 633, to image elastin, was excited with a 633 nm HeNe laser. Alexa Fluor 546 phalloidin, to image F-actin components, was excited with a 543 nm HeNe laser.

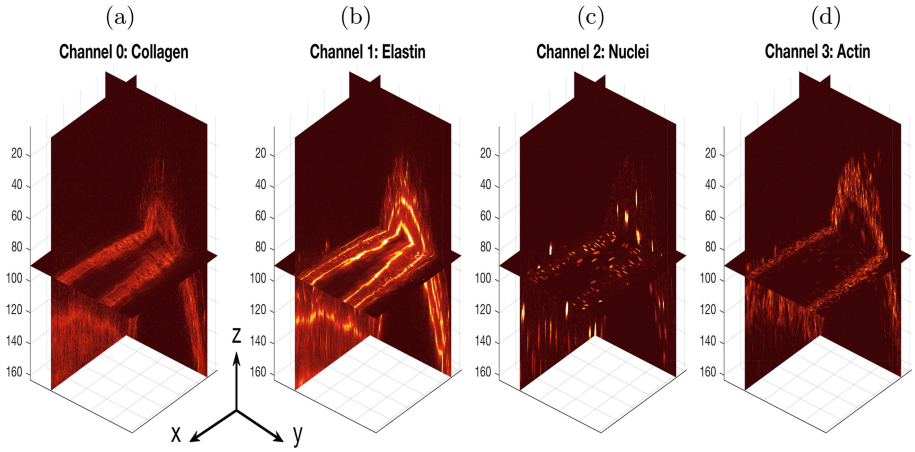

Fig. 1. Illustration of one representative artery and the four channels acquired under the following conditions: (a) subject to second harmonics to acquire collagen, (b) stained with Alexa633 to image elastin, (c) stained with DAPI to for cell nuclei, (d) stained with Phalloidin to for actin. Data is shown in 3 orthogonal planes, the horizontal xy is the acquired in the microscope and vertical planes (traversal yz to the artery on right and parallel xz on the left) are reconstructed. It can be noticed in (b) the presence of two laminae expressing Elastin and how these laminae locate as concentric regions. Another relevant observation is that the lines corresponding to the lamina in xy are getting closer towards the right side and closer to the yz plane, this indicates that the artery is not aligned with the plane. If the plane and artery were perfectly aligned, the lines should be parallel.

DAPI, to image nuclei, was excited with a multi-photon laser at 720 nm. Collagen was imaged via second-harmonic image generation using a multi-photon laser at 850 nm as previously described [5] (Fig. 1).

2.2 Methods

Alignment of the Arteries. Whilst care is taken at the position of the samples in the microscope, variations in alignment occur, especially in the *elevation* which is manifest in Fig. 2 in sets B and D. The data sets were thus aligned by rotating the data along the z axis (rotation of original images) and then a rotation along the y axis (axis perpendicular to the direction of the vessel). Once the vessel was oriented as close as possible to a cylinder aligned with the x axis, the maximum intensity projection over this axis was calculated. This projection (Fig. 3a) has a similar appearance to one yz plane as that of Fig. 2, but it compensates for any small variation along the artery.

Segmentation of the Laminae. To determine the edges of the internal and external laminae of the artery, a multiscale calculation of the Canny edges [11] was performed by increasing the variance of the Gaussian until an asymptotic

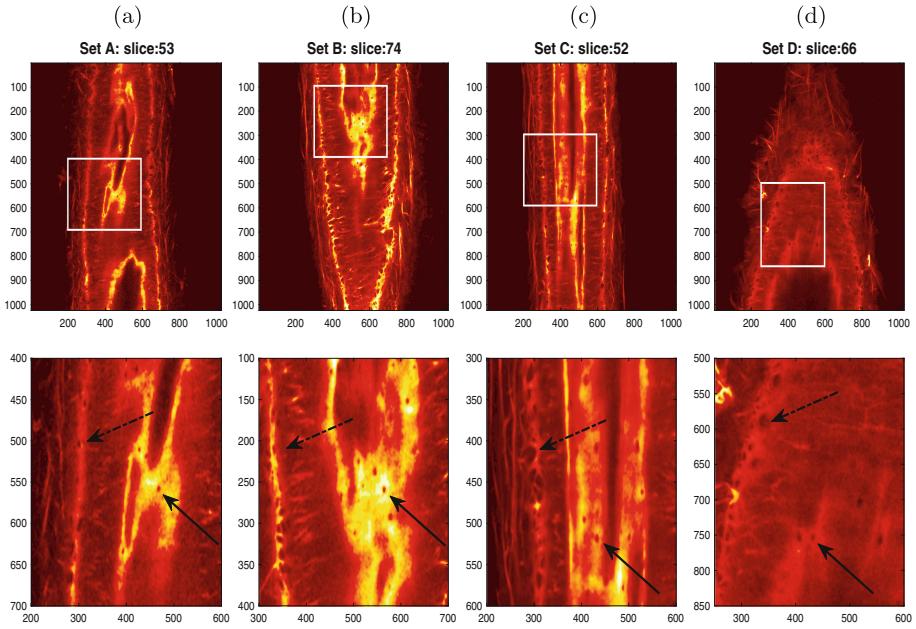

Fig. 2. Representative images of the IEL stained with Alexa633 that show the presence and variability of fenestrae in four different data sets. Regions of interest are denoted with a white rectangle and shown in the second row. Some fenestrae of the IEL are illustrated with solid arrows whilst structures of the EEL are indicated with dashed arrows. It is important to notice several points: Fenestrae appear as dark circular regions as compared with their surroundings, fenestrae-like structures can also be present in the EEL, but in general the fenestrae of the IEL are smaller in size, arteries are not always well aligned as shown in B and D where the arteries are tilted in opposite directions.

number of edges, ideally one for each side of the artery, was reached (Fig. 3a). When the top of the artery was too close to the edge of the field of view, the asymptotic number was 3 as the edge over the top was broken into two. The external edge presented considerable variability due to the nature of the EEL, therefore the segmentation of IEL was obtained from the dilation of the internal edge. To select the EEL, the dilated region was used to remove the intensity of the IEL. The regions corresponding to each of the laminae were further removed when the projections for each were calculated.

Projection to a Plane. The previous step identified the regions for the EEL and the IEL, but these were still distributed in a cylindrical shape over several dimensions, thus the next step was to project the intensities towards a single 2D plane. This was performed by a ray tracing from the central line of the assumed cylinder. Figures 3b, c illustrate both laminae in position with respect to the yz plane for one set, and Fig. 4 shows the maximum intensity projection of the IEL and EEL for the four data sets.

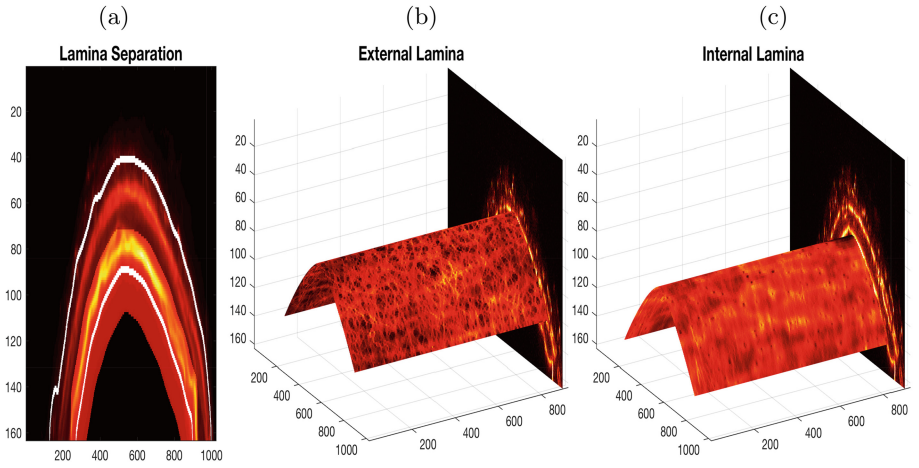

Fig. 3. Segmentation of the laminae of data set C. The maximum intensity projection along axis x towards the traversal plane are illustrated with white lines denoting the boundaries of the artery and the ROI of the internal lamina is highlighted with a brighter shade. On the right the EEL and IEL are illustrated on their position over the artery.

Segmentation of the Fenestrae. The fenestrae could be described as small, dark round regions surrounded by brighter pixels. Taking this characteristic into account, six segmentation algorithms were tested: (1) thresholding after a median filter was applied, (2) thresholding after median filter and morphological closing, (3) thresholding after a convolution with a Gaussian Kernel, (4) thresholding after finding peaks in the image, (5) detection of the fenestrae from the peaks of a Hough transform, (6) thresholding after convolution with a Laplacian of a Gaussian (L.O.G.).

Ground Truth. To validate the segmentation methods previously mentioned, three independent observers performed a manual delineation of the fenestra. Results are shown in the top row of Fig. 5 as colours (red, green, blue) assigned to each observer. The results illustrate the common intra-observer variability; regions selected by all 3 appear in white, with other colours as pairs or single selections.

Evaluation Metrics. Pixels were classified as true positives (TP Fenestrae segmented as Fenestrae), true negatives (TN Background segmented as Background), false positives (FP Background segmented as Fenestrae) and false negatives (FN Fenestrae segmented as Background). Then the accuracy was calculated as $(\mathrm{TP}+\mathrm{TN})/(\mathrm{TP}+\mathrm{TN}+\mathrm{FP}+\mathrm{FN})$ and the Jaccard Similarity index [12] was calculated as $(\mathrm{TP})/(\mathrm{TP}+\mathrm{FP}+\mathrm{FN})$.

Additionally, the number of fenestrae detected automatically and the numbers of the ground truth were compared.

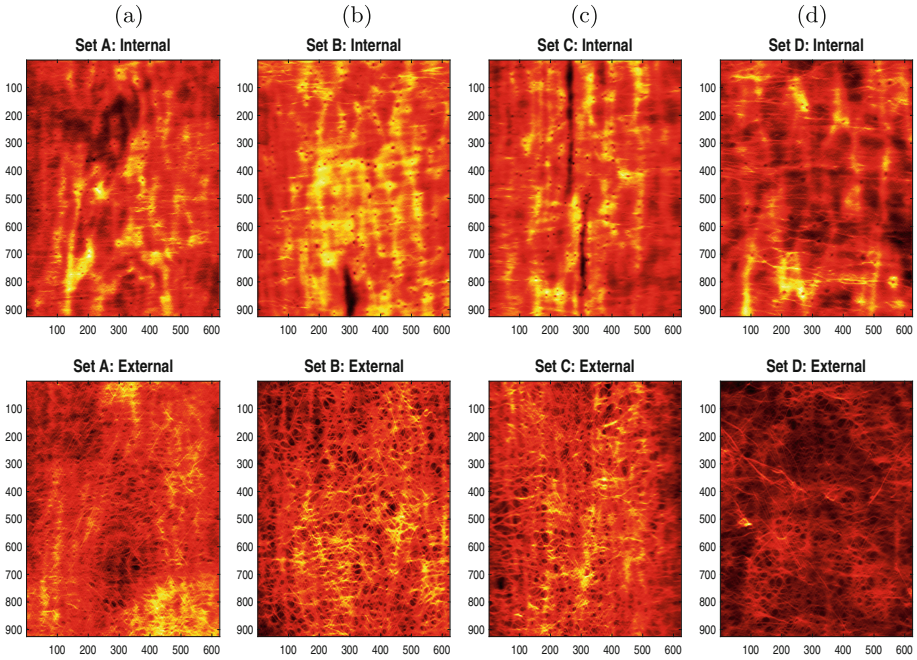

Fig. 4. Projected Internal and External laminae for the four representative cases of Fig. 2. Notice how the projections contain a considerable larger number of fenestrae to be analysed as compared with single slices. This is particularly important on the lower slices of the set (corresponding to the left and right edges of the images) as those fenestrae would be difficult to observe in horizontal planes. The EEL presents interesting structures that will be analysed in the future as it is beyond the scope of this paper.

3 Results and Discussion

For purposes of comparison, valid fenestrae were considered those regions selected by 2 or more observers, i.e. the three manual segmentations were added and the ground truth were all pixels with values greater than 1. These correspond to the yellow, magenta, cyan and white regions of Fig. 5. It should be noticed that this criterion is far from perfect as there were several regions that were detected by one single observer, particularly red regions in sets A and C, and green regions in set D. This procedure assumes that all the manual selections are equally likely and if only one observer is more careful or has a better understanding of the fenestrae, his or her observations could be removed by two less experienced ones. Any future work should have a more careful manual selection of fenestrae.

Six segmentation algorithms were tested with the four data sets displayed previously. Since there were large areas of background, the majority of pixels were allocated as TN and thus the accuracy measurements were rather high and

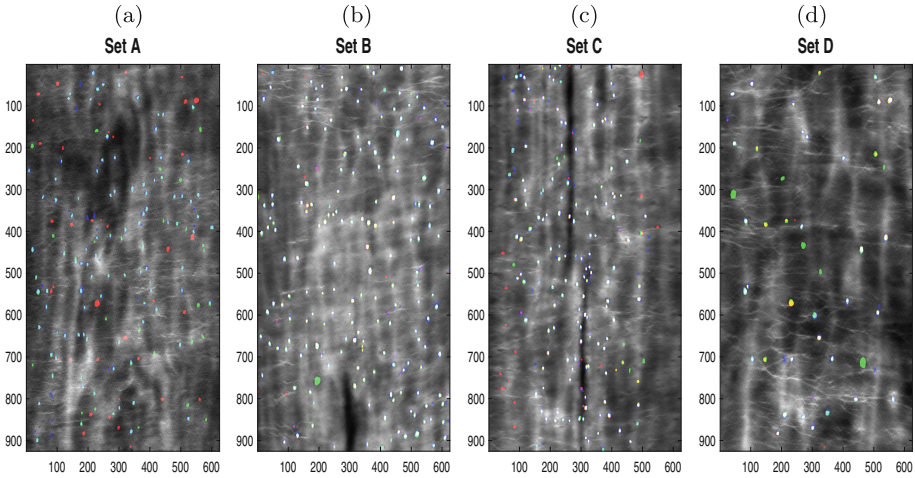

Fig. 5. Comparison of manual segmentation of 3 independent observers, red regions correspond to observer 1, green to 2, blue to 3, common selections correspond to 1 + 2 yellow, 1+3, magenta, 2+3 cyan, 1+2+3 white. It should be noticed the large variation of the observers. Regions where 2 or more observers coincided were considered as ground truth for classification. (Color figure online)

it was considered that the Jaccard would be a better indication of the algorithms. The results obtained were the following: (1) thresholding after a median filter was applied **37.2%**, (2) thresholding after median filter and morphological closing **19.4%**, (3) thresholding after a convolution with a Gaussian Kernel **34.3%**, (4) thresholding after finding peaks in the image **34.1%**, (5) detection of the fenestrae from the peaks of a Hough transform **34.0%**, (6) thresholding after convolution with a Laplacian of a Gaussian (L.O.G.) **45.58%**.

Overall, the classification accuracy obtained (pixelwise foreground/background) was in the range [98–99%] and Jaccard Index values (pixelwise intersection over union) in the range of [38–54%] for data sets A–D (Fig. 6), which are comparable to the variation of the manual classifications.

The algorithm that provided best results was performing a convolution with a Laplacian of a Gaussian kernel and then applying a threshold. The parameters of this last segmentation algorithm were subject to a sensitivity analysis by systematically varying the parameters of Laplacian of a Gaussian and the threshold. Optimal values corresponded to size = 13, variance = 4, threshold of 0.25%. It was noted that the algorithm was sensitive to the size of the kernel only for small kernels and for larger ones it remains fairly stable. The variability with the threshold displayed a shape similar to a Poisson distribution (Fig. 7a). A comparison of the number of fenestrae detected showed that the optimal results were obtained with the same range of parameters, with results of around 15% variation in the number of fenestra detected (Fig. 7b).

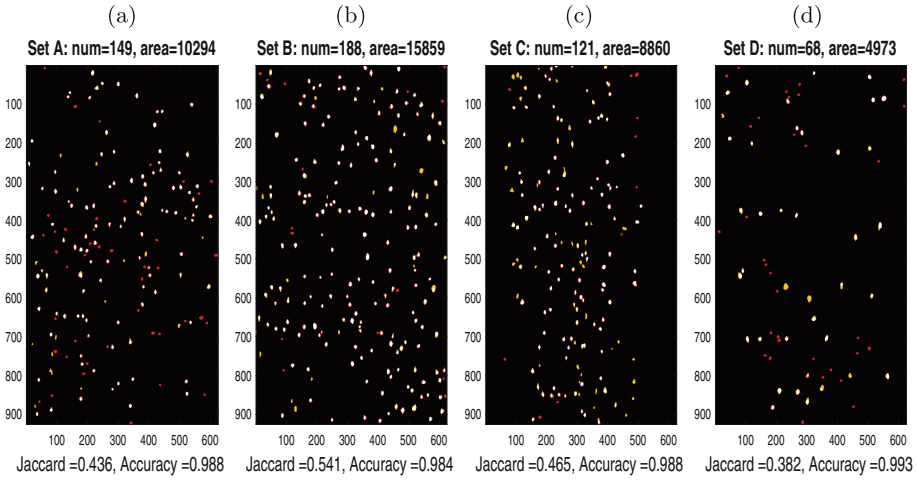

Fig. 6. Automatic segmentation: black = background, white = True positives, red = false positives, yellow = false negatives. Notice the difference between mesenteric arteries (A, B, C) and a femoral artery (D). (Color figure online)

The algorithms were then applied to analyse the arteries of the two groups: spontaneously hypertensive rat (SHR) and normotensive control (WKY) rats. WKY rats reported a higher number of fenestrae and fenestrae of larger areas (Fig. 8). These results are consistent in the number of fenestrae with previously published data [13] and our own previous experimental analyses made by visualisation and manual counting. The sizes correspond to range of sizes reported by [10] within the normal range (mean diameter $2.13 \pm 0.13\,\mu\text{m}$), and much smaller that the enlarged fenestrae (mean diameter $7.0 \pm 0.34\,\mu\text{m}$).

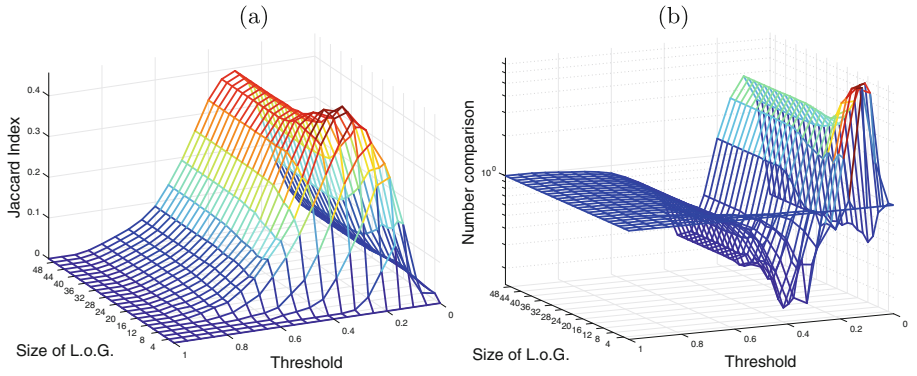

Fig. 7. Number and size of fenestrae showed statistical difference between WKY and SHR rats.

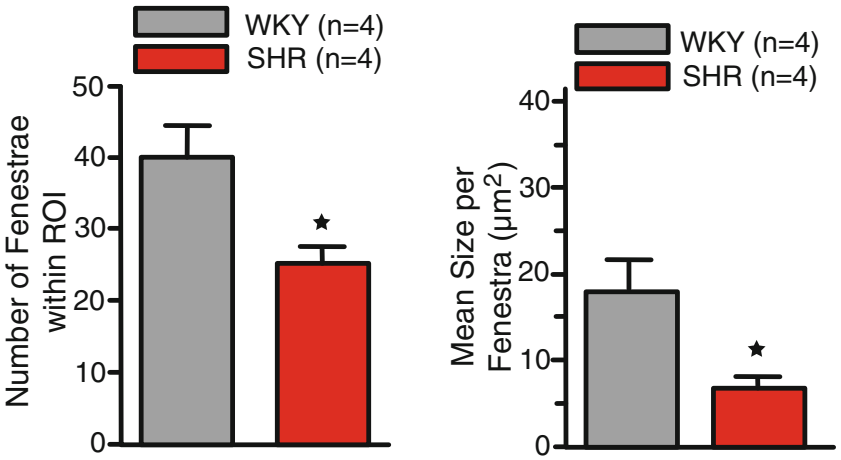

Fig. 8. Number and size of fenestrae showed statistical difference between WKY and SHR rats.

However, the calculations on the mean size of fenestrae were discordant between the two methods. Further analyses need to be performed to determine the source of variation in the measurement of fenestrae size.

Further analysis will focus also on the mean density of fenestrae, mean percentage area and shapes of the fenestrae. Another possible extension would be to compare fenestrae characteristics with age, as it has been reported in rabbits that fenestra increases dramatically with postnatal development [14].

References

1. Gerszten, R.E., Wang, T.J.: The search for new cardiovascular biomarkers. Nature **451**, 949–952 (2008)
2. Hedley, A.A., Ogden, C.L., Johnson, C.L., Carroll, M.D., Curtin, L.R., Flegal, K.M.: Prevalence of overweight and obesity among us children, adolescents, and adults, 1999–2002. JAMA **291**, 2847–2850 (2004)
3. Ramirez-Perez, F.I., et al.: Maternal hyperleptinemia increases arterial stiffening and alters vasodilatoy responses to insulin in adult male mice offspring. FASEB J. **30**(Suppl. 1), 721.8 (2016)
4. Pennington, K.A., et al.: Maternal hyperleptinemia is associated with male offsprings altered vascular function and structure in mice. PLOS One **11**(5), e0155377 (2016)
5. Bender, S.B., et al.: Regional variation in arterial stiffening and dysfunction in Western diet-induced obesity. Am. J. Physiol. Heart Circ. Physiol. **309**(4), H574–582 (2015)
6. Dzau, V.J., Gibbons, G.H.: Vascular remodeling: mechanisms and implications. J. Cardiovasc. Pharmacol. **21**(Suppl 1), S1–5 (1993)
7. Movat, H.Z., Fernando, N.V.P.: The fine structure of the terminal vascular bed I. Small arteries with an internal elastic lamina. Exp. Mol. Pathol. **2**(6), 549563 (1963)

8. Foote, C.A., et al.: Arterial stiffening in western diet-fed mice is associated with increased vascular elastin, transforming growth factor-β and plasma neuraminidase. Front. Physiol. **7**, 285 (2016)
9. Masuda, H., Zhuang, Y.-J., Singh, T.M., Kawamura, K., Murakami, M., Zarins, C.K., Glagov, S.: Adaptive remodeling of internal elastic lamina and endothelial lining during flow-induced arterial enlargement. Arterioscler. Thromb. Vasc. Biol. **19**(10), 22982307 (1999)
10. Campbell, G.J., Roach, M.R.: Fenestrations in the internal elastic lamina at bifurcations of human cerebral arteries. Stroke **12**(4), 489496 (1981)
11. Canny, J.: A computational approach to edge detection. IEEE Trans. PAMI **8**(6), 679–698 (1986)
12. Jaccard, P.: Étude comparative de la distribution florale dans une portion des Alpes et des Jura. Bull. Soc. Vaud. Sci. Nat. **37**, 547–579 (1901)
13. Briones, A.M., et al.: Role of elastin in spontaneously hypertensive rat small mesenteric artery remodelling. J. Physiol. (Lond.) **552**(Pt 1), 185–195 (2003)
14. Wong, L.C.Y., Langille, B.L.: Developmental remodeling of the internal elastic lamina of rabbit arteries: effect of blood flow. Circ. Res. **78**(5), 799805 (1996)